Measurement of the skin layer in the drying process of a polymer solution

Yuji Shimokawa
Department of Applied Physics, School of Engineering, The University of Tokyo, 7-3-1 Hongo, Bunkyo-ku, Tokyo 113-8656, Japan

Tadashi Kajiya
Laboratoire MSC, UMR 7057, CNRS, Université Paris Diderot, Bâtiment Condorcet, 10 rue Alice Domon et Léonie Duquet, 75205 Paris Cedex 13, France

Keiji Sakai
Institute of Industrial Science, The University of Tokyo, 4-6-1 Komaba, Meguro-ku, Tokyo 153-8505, Japan

Masao Doi
Department of Applied Physics, School of Engineering, The University of Tokyo, 7-3-1 Hongo, Bunkyo-ku, Tokyo 113-8656, Japan
(Received 23 July 2011; revised manuscript received 5 October 2011; published 4 November 2011)

When a polymer solution is dried in air, a polymer-concentrated region, called a "skin" layer, often appears near the surface. In this paper, an experimental method is proposed for detecting the initial process of the formation of the skin layer. An electric field is applied on the surface of polymer solutions by a wedge-type "electric field tweezers," and the dynamic response of the surface profile is measured by an optical lever technique. Our experiments and theory indicate that when a skin layer is formed, (i) the slow relaxation process appears in the time domain and (ii) the long-persisting dip region appears in the surface profile. A parameter to quantify the difference of the surface response is proposed in this paper.

DOI: 10.1103/PhysRevE.84.051803 PACS number(s): 61.41.+e

I. INTRODUCTION

Drying of polymer solutions and colloid dispersions can be seen in our daily life, such as in the drying of inks, paints, glues, etc. The drying process is also very important in many industrial applications, for instance the fabrication of functional polymer films, inkjet printing, and wet coating. As more precision and higher throughput are required in these technologies, understanding and controlling the drying process remains an important issue [1], and there are still many unsolved issues.

One example of such an issue is the "skin" formation in the drying of polymer solutions. When the solvent in polymer solutions evaporates rapidly, it leaves a polymer-concentrated region near the surface and creates a "skin" layer near the surface [2,3]. It has been said that once the skin phase is formed, it causes many problems in industrial products, including buckling instability [2,3], bubble appearance, and a decrease in the evaporation rate [4], but the exact relation between skin formation and these problems is not well understood.

de Gennes [4] gave a theoretical analysis for the formation of a glassy phase, which he called the "crust" near the surface. Okuzono *et al*. [5–7] proposed a model for the skin formation process and proposed a criterion for the skin layer to be formed. Pauchard *et al*. [2,3] analyzed the buckling of the glassy layer induced by drying. On the other hand, there are few experimental studies for skin layers. One reason for this is that invasive measurement of the skin layer is difficult. Since the skin layer is thin and adhesive, mechanical contact between the probe and the sample surface destroys it. Ludwig *et al*. [8] developed a technique of Raman confocal microscopy to measure the time variation of the vertical concentration profile, but this method is limited to thin films, for which a skin layer is not formed.

We have developed a technique to detect the skin layer mechanically without contacting the surface of the drying sample. We combined the "electric field tweezers" developed by Sakai *et al*. [9] with the optical lever technique using parallel-lined laser beams, and we measured the response of polymer solutions to the dielectric force applied on the surface. The method allows us to detect the formation of the skin layer in the early stage. In this paper, we describe the experimental method, and we report a few examples of the experimental data.

II. EXPERIMENT

Figure 1(a) shows the principle of our system. A liquid sample is spread in the bottom surface of a glass petri dish of diameter 65 mm and depth 15 mm. The thickness of the liquid is between 2 and 5 mm. A metal blade of length 15 mm is placed 1 mm above the sample with its edge set horizontally. The blade is connected to a function generator (FG 120, Yokogawa Electric Co., Japan), an oscilloscope (DL1740E, Yokogawa Electric Co., Japan), and a high-voltage amplifier (HOPS-3P1, Matsusada Precision Inc., Japan). When a high voltage (100 V–1 kV) is applied to the blade, the electric field generated at the edge of the blade pulls up the sample surface.

The displacement of the sample surface is measured by the optical lever technique. A He-Ne laser is expanded by a beam expander and focused by a cylindrical lens to form a laser sheet, which is then passed through a grid made of transparent film with the grid pattern printed in black (spacing and linewidth are both 0.3 mm). The obtained parallel-lined laser beams are shone on the sample surface, and the reflected beams are projected on the screen placed above the sample. If the sample surface is flat, the bright points on the screen are equally spaced. If the sample surface is curved, the bright points on the screen are displaced from the original position. The screen

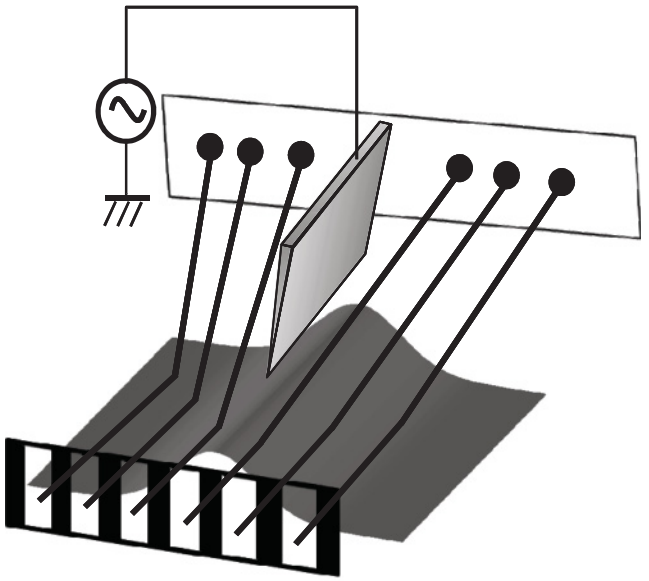

(a)

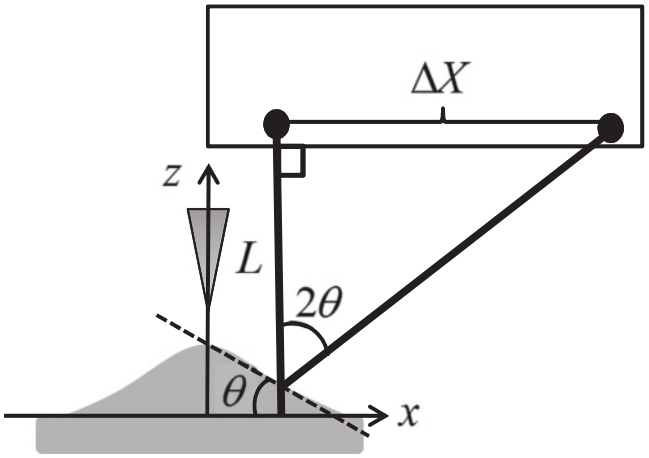

(b)

FIG. 1. (a) Experimental setup. The surface deformation induced by the dielectric force is measured by parallel-lined laser beams. (b) The relation between the shift of the bright point ΔX and the inclination of the surface $\mathrm{d}\zeta/\mathrm{d}x$.

image is captured by a charge-coupled device (CCD) camera, and the positions of the bright points are obtained by image analysis. The deformation of the sample surface was calculated from the displacement of the bright points ΔX as follows.

We consider the orthogonal coordinate shown in Fig. 1(b), where the x axis is taken horizontally in the sample surface. Let $\zeta(x)$ be the vertical displacement of the sample surface at coordinate x. If the sample surface is not horizontal, the direction of the laser beam changes after the reflection, and thus the position of the bright point on the screen is shifted to a distance ΔX. For a small change of the surface from the horizontal line, ΔX is proportional to $\mathrm{d}\zeta/\mathrm{d}x$,

$$\frac{\mathrm{d}\zeta}{\mathrm{d}x} = -\frac{\Delta X}{2L}, \tag{1}$$

where L is the distance from the sample surface to the bright points in a vertical direction (L corresponds to the arm length of the optical lever). In this study, L is set to about 40 mm. The surface deformation is calculated by integrating Eq. (1) numerically. In this method, the time resolution is limited by the speed of the CCD camera. In the present experiments, we used the usual frame rate (10 frames per second).

The petri dish containing the sample is placed on an electric balance (TE1520S, Sartorius Mechatronics Japan), and the sample weight is measured simultaneously with the surface response in the whole process of drying.

A step electric field is used for the measurement. We apply a constant field at time $t = 0$, hold it for some time (typically 10 s), and switch it off, and we measure the time variation of the surface profile. (In practice, we apply an alternating electric field with frequency 1 kHz instead of dc field. This is to avoid an unwanted charge up of the surface. Since this frequency is much higher than the characteristic frequency of the surface response, we can ignore the ac character of the field and regard the field as static.) All measurements are conducted at room temperature (23 °C).

III. TEST OF THE SYSTEM

To check the performance of the system, we measure the surface profile and the dynamic response of the surface for several simple fluids.

A. Equilibrium surface profile

Figure 2 shows the equilibrium profiles of the sample surface under constant electric field. The surface deformation of ethanol, glycerin, and silicone oil is plotted as points in Fig. 2. Solid lines represent theoretical curves, which are obtained as follows.

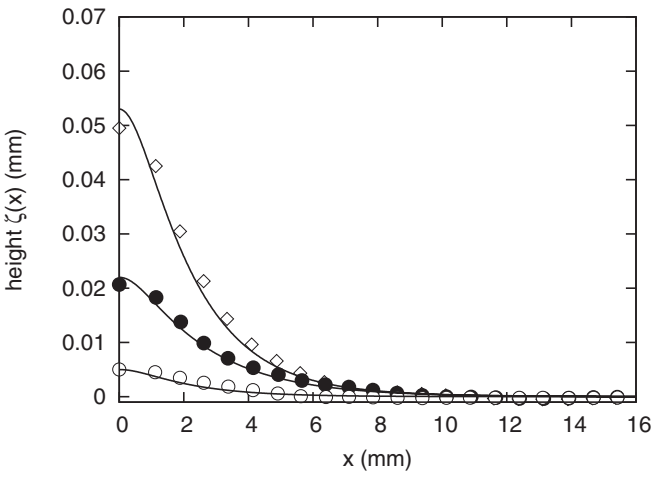

FIG. 2. The equilibrium surface profiles of ethanol (◇), glycerin (●), and silicone oil (○) under the applied voltage of 375 V. The sample thickness was 5 mm. The solid lines represent the theoretical curves explained in the text.

Consider a force $P_M(x)$ applied normal to the surface. The surface profile $\zeta(x)$ at equilibrium is obtained by solving the following force balance equation [9]:

$$-\gamma \frac{\mathrm{d}^2\zeta}{\mathrm{d}x^2} + \rho g \zeta = P_M(x), \tag{2}$$

where ρ and γ are the density and surface tension of the liquid, and g is the gravity acceleration. To calculate $P_M(x)$, we regard the blade electrode as a line charge that has a constant charge density and a finite length ℓ, and we use the image charge method. The details of the calculation are explained in Appendix A, and the result is

$$P_M(x) = \frac{C}{(x^2+a^2)^2} \frac{x^2+\varepsilon_r a^2}{x^2+a^2+(\ell/2)^2}, \tag{3}$$

where ε_r is the dielectric constant of the sample relative to that of air, a is the distance between the sample surface and the edge of the electrode, and C is a constant that is proportional to the square of the line charge density.

Given $P_M(x)$, Eq. (2) is easily solved for $\zeta(x)$:

$$\zeta(x) = \int_{-\infty}^{\infty} \mathrm{d}x' \frac{1}{2\gamma} \frac{\mathrm{e}^{-\kappa|x-x'|}}{\kappa} P_M(x'), \tag{4}$$

where

$$\kappa \equiv \sqrt{\rho g/\gamma} \tag{5}$$

is the inverse of the capillary length.

The solid lines in Fig. 2 show the theoretical curves of Eq. (4), where κ was calculated by the known values of γ for each sample and C was regarded as a fitting parameter. The theoretical lines are in good agreement with the measured surface profiles for each sample.

B. Dynamic response

Figure 3 shows the surface response of silicone oil (10 Pa s) when a constant electric field is switched on at $t = 0$ s and switched off at $t = 10$ s. The displacement of the top height, i.e., the value of $\zeta(x,t)$ at $x = 0$, is plotted against time in Fig. 3(a). The snapshots of the surface profile during the transient response are shown in Figs. 3(b) and 3(c). The vertical displacement of the sample surface is very small, of the order of several tens of micrometers.

Figure 3(a) indicates that the top of the sample surface behaves like a step response of the Voigt model, where the restoring force is the surface tension and the friction is the bulk viscosity. The position of the top height reaches equilibrium after the electric field is applied, and decays exponentially to the original position after the electric field is switched off. We conduct the measurements for silicone oils having viscosities 5, 10, 50, and 100 Pa s, and we obtain the characteristic relaxation time τ, which is the time at which the top height decays to half of the value before the electric field is switched off. Figure 4 shows this relaxation times plotted against the viscosity. It is seen that the relaxation time is proportional to the sample viscosity, as expected from the dimensional analysis for Newtonian fluid.

This test demonstrates that our system can accurately measure the dynamic response of the sample profile.

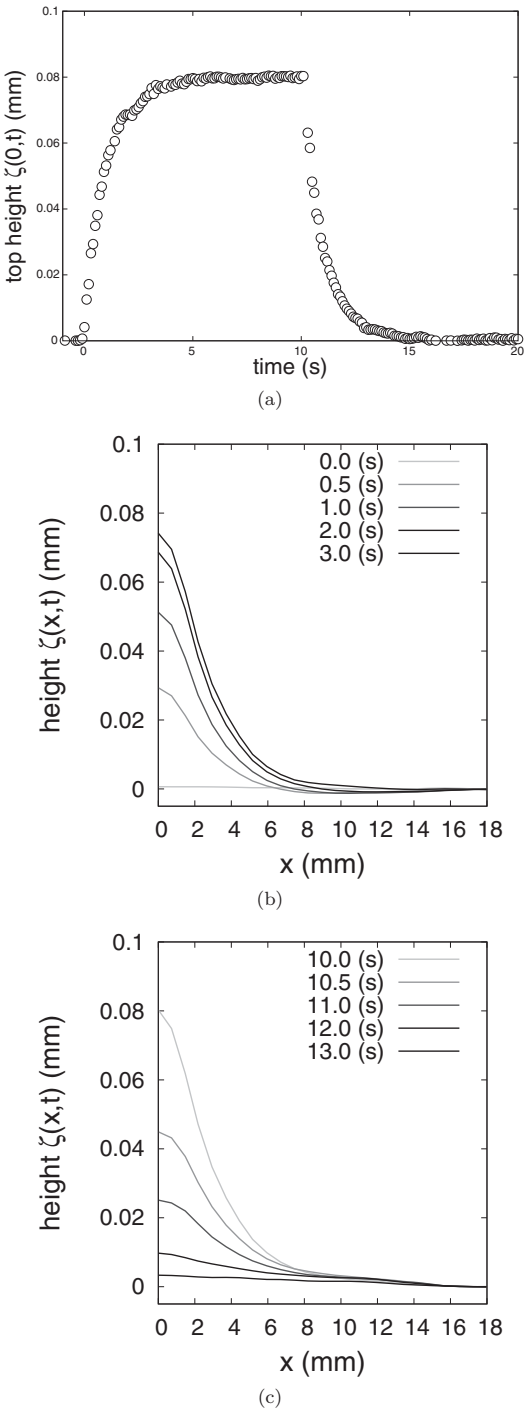

FIG. 3. Time variation of the surface profile $\zeta(x,t)$. (a) Time dependence of the top height $\zeta(0,t)$ of silicone oil (10 Pa s). The applied voltage was 1.5 kV and the sample thickness was 5 mm. (b) Time variation of surface profile $\zeta(x,t)$ when the electric field is switched on. (c) Time variation of surface profile $\zeta(x,t)$ when the electric field is switched off.

IV. RESULTS FOR A POLYMER SOLUTION

Next we apply our system to study the drying process of polymer solutions, the solution of poly methyl methacrylate (PMMA; Sigma-Aldrich Co., USA; typical

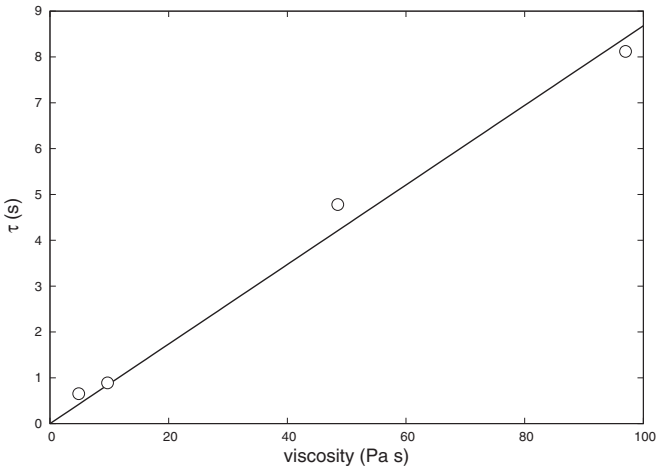

FIG. 4. Time constant of the surface response of silicone oil plotted against the viscosity. The solid line shows the linear relation between the relaxation time τ and the viscosity η.

M_w996 000 g/mol) in acetone (Junsei Chemical Co., Ltd., Japan; T_b56 °C).

A. Measurement of the dynamic response

Figure 5 shows the time variation of the sample weight and the average polymer concentration calculated from the weight. It is seen that the evaporation rate is almost constant for about 60 min after the drying is started, and decreases quickly after that. The average polymer concentration increases with an S-shaped curve.

Figure 6 shows the step response of the top height when the average concentration reaches 13%, 15%, and 16% in the drying process. The data of 14% are not shown in Fig. 6 to avoid a bothersome overlapping of points. When the average concentration is 13%, the behavior of the top height is similar to that of pure viscous fluid shown in Fig. 3(a). This behavior can be fitted by a single exponential curve. When the average concentration reaches 15% and 16%, the surface response is slowed down, and the curves cannot be fitted by a single exponential curve anymore.

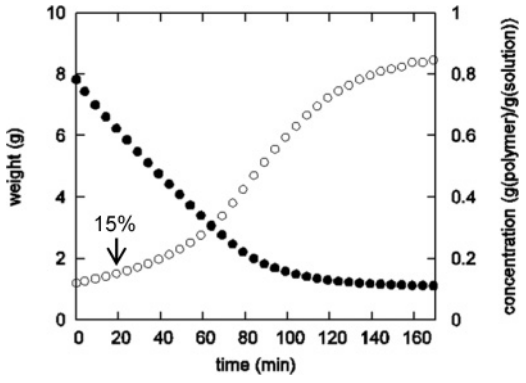

FIG. 5. Time variation of the weight (●) of PMMA/acetone solution and PMMA concentration (○) in the drying process for Fig. 6. The arrow indicates the time at which the average concentration reached 15%.

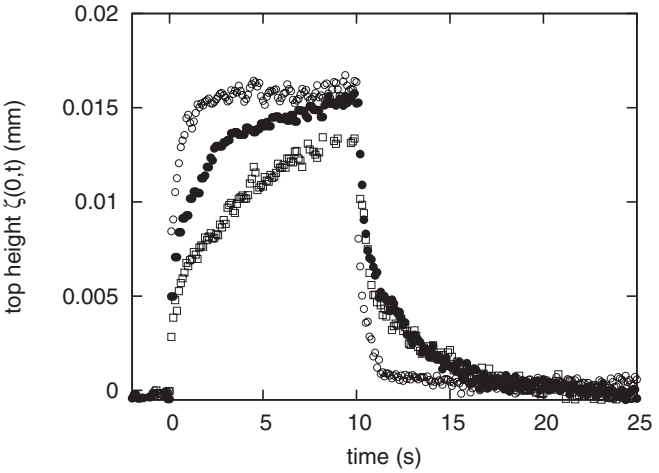

FIG. 6. Time dependence of the top height $\zeta(0,t)$ of PMMA/acetone solution in the drying process. Different symbols indicate the results when the average concentration reaches 13% (○), 15% (●), and 16% (□). The applied voltage was 225 V and the initial thickness of the sample was 3 mm.

The slowing down of the response for the concentrated samples is not surprising because polymer solutions become more viscous with the increase of polymer concentration. An important point in Fig. 6 is that the shape of the response curve changes as the drying proceeds. For the sample of 15% and 16%, the height $\zeta(0,t)$ first increases as quickly as the sample of 13%, but then the increase is slowed down. This point is demonstrated more clearly by the following experiment.

1. Comparison between the drying solutions and the uniform solutions

Figure 7 shows the comparison of the response of two samples that have the same average concentration of 15%, but are prepared in a different way. One sample, which we shall refer to as the drying sample, is made by drying the sample of 12% solution for about 20 min (the precise time is determined from the weight of the sample). The other sample, which we shall refer to as the uniform sample, is made by mixing the polymer and the solvent homogeneously. In the measurement of the latter sample, the sample is placed in the acetone vapor bath. Although the average concentrations of these samples are the same, the polymer distributions in a vertical direction are different.

Figure 7 indicates the clear difference between these samples. Figure 7(a) shows the time variation of the top height. The top height of the uniform sample behaves more like a normal viscous fluid than the drying sample. Figures 7(b) and 7(c) show the time variation of the surface profile for the two samples after the electric field is switched on. It is seen that after the electric field is switched on, there appears a dip region, where $\zeta(x,t)$ is negative. The dip region maintains a relatively long time for the drying sample [Fig. 7(b)], while it quickly disappears for the uniform sample [Fig. 7(c)].

To quantify the surface response of the drying sample and the uniform sample, we defined a dip parameter D as the ratio of the area of dip region $S^{(-)}$ to the area of bump region

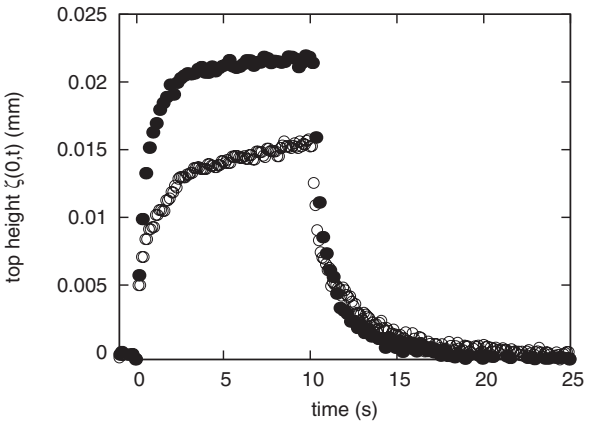

(a)

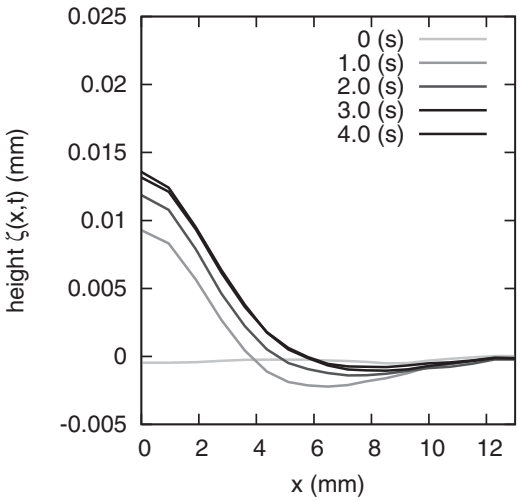

(b)

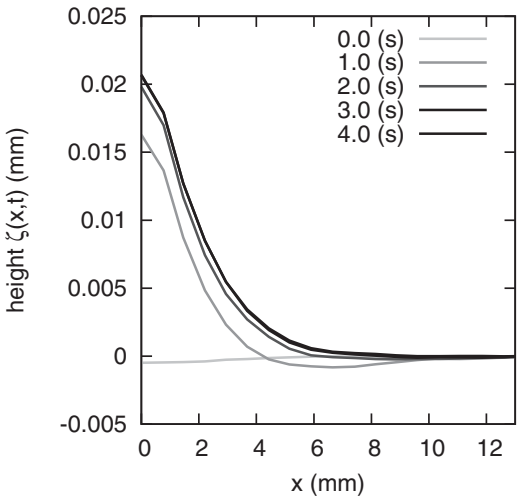

(c)

FIG. 7. Comparison of the dynamic surface response of PMMA/acetone solution between the drying sample and the uniform sample, both having the same average polymer concentration of 15%. (a) Time variation of the top height $\zeta(0,t)$ for the drying sample (○) and the uniform sample (●). (b) Time variation of the surface profile $\zeta(x,t)$ for the drying sample. (c) Time variation of the surface profile $\zeta(x,t)$ for the uniform sample. The magnitude of the applied voltage was 225 V.

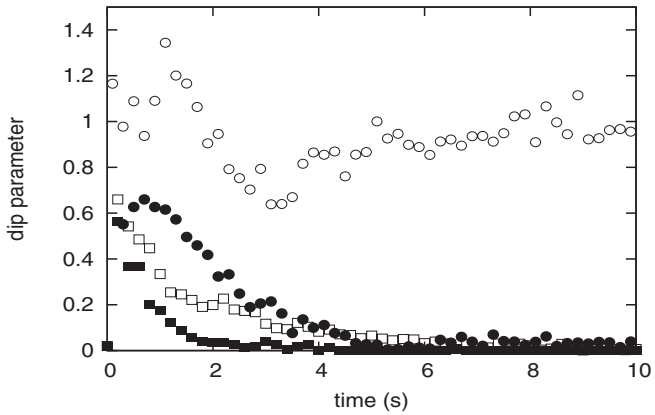

(a)

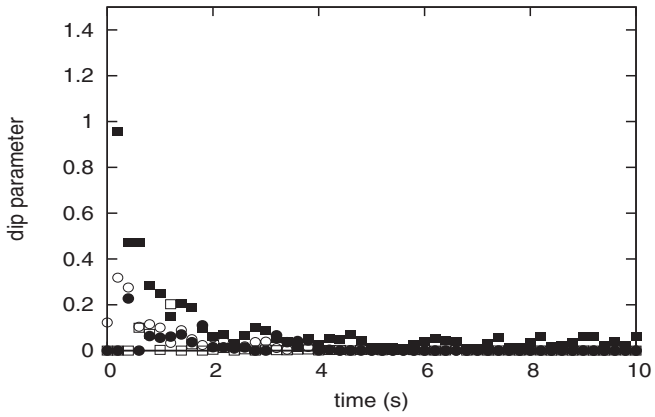

(b)

FIG. 8. Dip parameter of PMMA/acetone solution is plotted against the elapsed time after the electric field is switched on for the drying sample (a) and for the uniform sample (b). In both figures, symbols represent the average concentration 13% (■), 14% (□), 15% (●), and 16% (○). The applied voltage was 375 V and the initial thickness of the sample was 3 mm for (a) and 2.5 mm for (b).

$S^{(+)}$, i.e., $D \equiv |S^{(-)}/S^{(+)}|$. $S^{(+)}$ and $S^{(-)}$ are defined by the following equations:

$$S^{(+)} = \int_0^{x_0} dx\zeta(x,t), \tag{6}$$

$$S^{(-)} = \int_{x_0}^{x_1} dx\zeta(x,t), \tag{7}$$

where x_0 is the position at which the surface profile $\zeta(x,t)$ crosses over the horizontal axis and x_1 is the edge of the surface profile.

Figure 8 shows the time dependence of the dip parameter of the drying sample [Fig. 8(a)] and that of the uniform sample [Fig. 8(b)] in other concentrations. The figure shows the difference in the behavior of the dip parameter more clearly. In the uniform sample, the dip parameter disappears within about 2 s for all concentrations, while in the drying sample, the dip parameter persists much longer. In the sample of 15%, the dip parameter even increases in a short time, taking a peak at 1 s, and then decreases. In the sample of 16%, the dip region remains for more than 10 s. These results indicate that

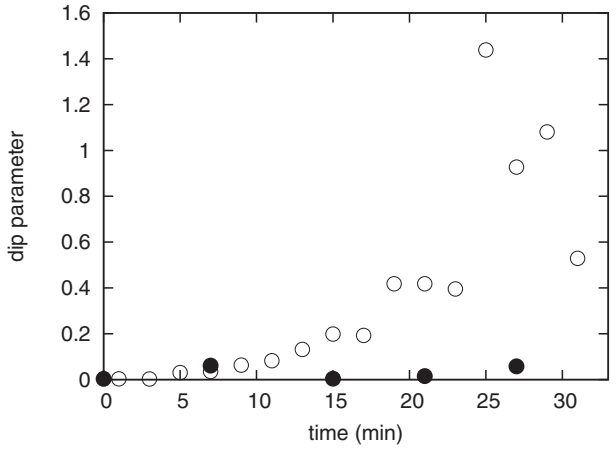

FIG. 9. Dip parameter of PMMA/acetone solution taken 2 s after the electric field is switched on is plotted against the time of drying by (○). For the sake of comparison, the results for the uniform sample are also plotted in the figure by (●).

the dip parameter is quite sensitive to the development of the concentration gradient in a vertical direction.

The dip parameter we have defined is an empirical parameter. In the following section, we shall give a qualitative explanation for why a long-persisting dip region appears for a liquid film with skin layers. At present, however, there is no simple model for the time variation of the dip parameter. Nevertheless, the dip parameter seems to be a useful parameter to distinguish the liquid film with and without the skin layers.

Figure 9 shows the time variation of the dip parameter in the drying process. Here the dip parameter at 2 s after the electric field is applied is plotted against the drying time by open circles. For comparison, the dip parameter of uniform samples of corresponding concentration is shown by filled circles. It is seen that the dip parameter of the drying sample starts to deviate from zero at around 10 min after the drying is started, and increases monotonically as time goes on. (We could not obtain the data after 35 min because the sample surface became rough and scattered the laser beam irregularly.) On the other hand, the dip parameter of the uniform sample remains almost zero in this concentration range.

These results indicate that an indication of the skin layer appears at a rather early stage, where the drying rate is almost constant.

V. DISCUSSION

We have seen that the liquid film that is considered to have a skin layer shows responses that are quite different from those of the normal viscous liquid film. The skin layer is a concentrated region of polymers, and is considered to have a pronounced elasticity (or viscoelasticity, to be more precise). Although the precise characterization of the skin layer is not possible using the present method, we can make a model for the skin layer and analyze the response of the model.

As the simplest model, we assume that the skin is a very thin elastic membrane with a surface elastic constant S and the bulk liquid is a viscous liquid of viscosity η. The surface elastic constant S is defined as the ratio between the force acting in the

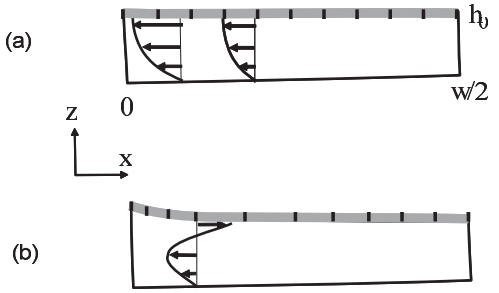

FIG. 10. Time variation of the flow profile in a liquid film covered with an elastic membrane when an electric field is switched on. (a) When the field is switched on, the fluid flows from the edge to the center and compresses the membrane in the center. (b) As time goes on, the elastic restoring force of the layer induces a back flow and slows down the fluid flow.

membrane per unit length and the strain of the membrane [see Eq. (B4)], and has the dimension of the surface tension. If the membrane is assumed to be a homogeneous elastic material with Young's modulus E, S is given by Eb, where b is the thickness of the membrane.

Figure 10 explains the response of such a system when the dielectric force $P_M(x)$ is applied on the surface. Since the dielectric force causes a flow from the edge to the center, as shown in Fig. 10(a), the membrane in the center is compressed. Accordingly, the compressed membrane tends to push back the flow from the center to the edge, as shown in Fig. 10(b). This explains the slowing down of the rise at the center shown in Fig. 6. Detailed analysis of this model can be done by using the lubrication approximation, and is described in Appendix B.

We have conducted a simulation for the time variation of the surface profile based on the model, and the results are explained below.

Figure 11 shows the time variation of the surface height at the center $\zeta(0,t)$ when the field is switched on at $t = 0$ and switched off at $t = 10$ s. Physical constants used in the simulation are taken from the experimental values and are given in the caption. The elastic constant S is not known, and we conducted a calculation varying S. In Fig. 11, we have shown only two curves, namely the curve for a skin-free film ($S = 0$) and the curve for a skin layer with a surface elastic constant of $S = 0.05$ N/m. This is due to the following reason.

The simulation indicates that with the increase of S, the response curve deviates from the curve of $S = 0$. The deviation becomes apparent when S becomes comparable with the surface tension γ. When S becomes much larger than γ, the curve approaches an asymptotic form, the curve for the film with an inextensible membrane. The value $S = 0.05$ N/m corresponds to the curve when the apparent deviation starts to saturate. We did not try to fit the simulation results with experimental curves since the model considered here ignores the thickness and the bending elasticity of the skin layer.

Despite the limitation of the model, the results of the simulation agree qualitatively with experiments. When there is a skin layer, the surface rising is slowed down. This is due to the back flow explained in Fig. 10(b). The compression of the skin layer in the center creates a back flow and slows down the rise of the center. The same mechanism is acting when the

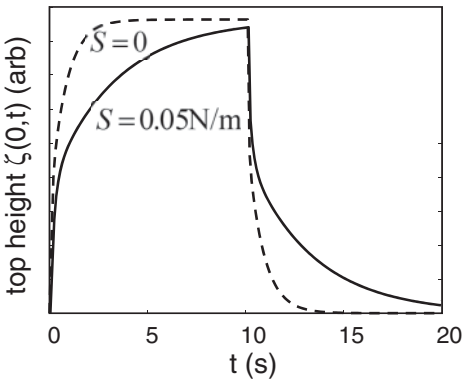

FIG. 11. Time variation of top height $\zeta(0,t)$ of liquid film without skins (dashed line) and with skins (solid line). Other parameters used in the calculations are $\eta = 1$ Pa s, $\gamma = 24$ mN/m, and $w = 3$ cm.

field is switched off. When the center is falling, the skin layer in the center is stretched, and the back flow tends to pull the outer part to the center, again slowing down the relaxation.

Figure 12 shows the time variation of the surface profile when the field is switched on. The top of Fig. 12 shows the profile of a liquid film without skins, while the bottom of Fig. 12 shows the result for liquid with skins of the surface elastic constant $S = 0.05$ N/m. Clearly the same trends as in experiments are seen in these figures. In the liquid without skins, the dip quickly disappears, while in the liquid with skins, the dip persists much longer. It is seen that the position of the minimum is pushed outward. This is again due to the back flow.

Figure 13 shows the time variation of the dip parameter obtained by the simulation. The dip parameter takes a sharp peak in a short time (less than 0.2 s). In the case of no skins, the dip parameter decreases monotonically, while in the presence of skins, the dip parameter shows the second local maximum.

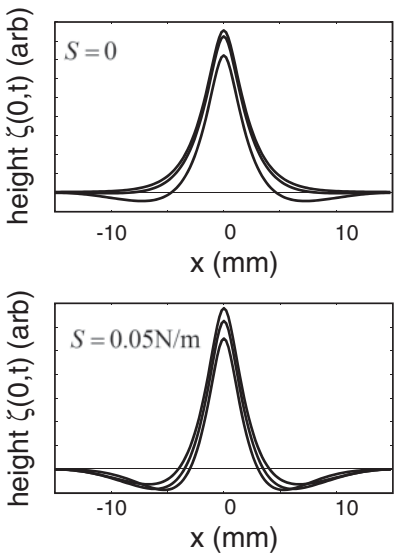

FIG. 12. Time variation of the surface profile $\zeta(x,t)$ at time $t =$ 1,2,3 s after the electric field is switched on. Top: without skin; bottom: with skin.

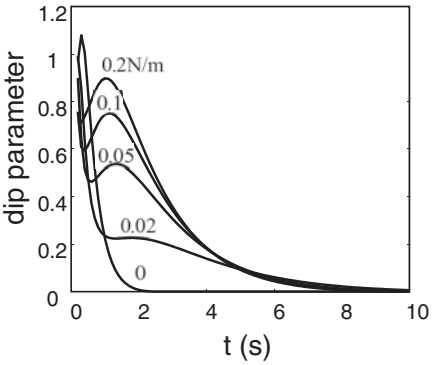

FIG. 13. Time variation of the dip parameter for various values of the surface elastic constant S.

This local maximum of the dip parameter is caused by the back flow due to the surface elasticity.

Figure 14 shows the dip parameter at time $t = 1.5$ s after the field is switched on plotted as a function of the surface elastic constant S. The dip parameter at this time is increased with the increase of the surface elasticity, i.e., the thickness of the elastic layer.

VI. CONCLUSION

We developed a technique of measuring the mechanical property of a liquid surface without contacting the surface. In this method, the surface deformation caused by the dielectric force is detected by an optical lever technique using parallel-lined laser beams. This method enables us to measure the dynamic surface response of polymer solutions in the drying process.

We applied this method to the PMMA/acetone solution in the drying process, and we observed a singular behavior different from the uniform sample. In the drying sample, a long-persisting dip region appears.

To quantify the characteristics of the dip region, we proposed the dip parameter and demonstrated that it effectively reflects the difference between the drying sample and the uniform sample. We also conducted a theoretical analysis and we have shown that a similar difference exists between the fluid film and the fluid film coated with a thin elastic membrane. We have also shown that the model reproduces the experimental results qualitatively. This analysis indicates

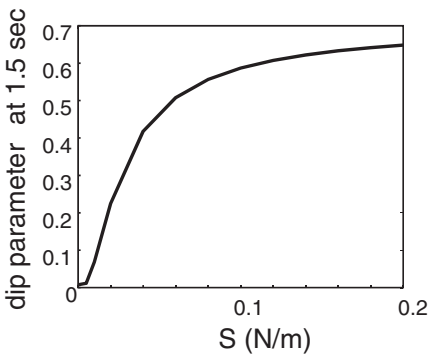

FIG. 14. Dip parameter at time 1.5 s after the electric field is switched on is plotted against the surface elastic constant S.

that the distinction between the fluid film with the elastic membrane and that without the membrane becomes apparent when the surface elastic constant S becomes comparable with the surface tension of the fluid. Therefore, we can estimate S to be of the order of the surface tension 10^{-2} N/m. Since the surface elastic constant is given by Eb (E and b being Young's modulus and the thickness of the membrane, respectively), we conjecture that the thickness of the skin we are measuring is of the order of 1–10 μm [assuming that Young's modulus of the skin layer is of the order of the plateau modulus of polymer solutions (10^3–10^4 Pa)]. Although further study is needed to confirm this conjecture, this result is reasonable.

These results indicates that our method is useful for detecting the appearance of the skin layer. The method does not tell us the detailed nature of the skin layer (such as the concentration profile in the layer and rheological properties), but we believe that the present technique is useful for studying the process of skin formation in the drying process of polymer solutions.

ACKNOWLEDGMENTS

The authors would like to thank T. Okuzono (Nagoya City University), Y. Sumino (Aichi University of Education), T. Yamaguchi, and S. Arai (The University of Tokyo) for useful discussions, and S. Mitani, T. Hirano, and T. Nagashima (IIS, The University of Tokyo) for their help in the experiment.

APPENDIX A: DERIVATION OF THE DIELECTRIC FORCE

To obtain the explicit representation of the dielectric force, we used the method of image charges. Suppose that the line charge with the charge density λ and the length ℓ is placed along the y axis. The sample surface is in the xy plane and the center of the line charge is placed $(x,y,z) = (0,0,a)$. The potential Φ, which is created by the line charge, is

$$\Phi(x,y,z) = \int_{-\ell/2}^{\ell/2} \mathrm{d}y' \frac{\lambda}{4\pi\varepsilon_0} \frac{1}{\sqrt{x^2+(y-y')^2+(z-a)^2}}, \tag{A1}$$

where ε_0 is the dielectric constant of the vacuum. Note that we regarded the dielectric constant of the air as that of the vacuum. Considering the image charges and the boundary condition in the xy plane, the electric field in the sample with the dielectric constant ε is given by

$$E_x|_{z=0} = \frac{\lambda}{2\pi r^2}\frac{1}{\varepsilon+\varepsilon_0} \times \left\{ \frac{x(y+\ell/2)}{\sqrt{r^2+(y+\ell/2)^2}} - \frac{x(y-\ell/2)}{\sqrt{r^2+(y-\ell/2)^2}} \right\}, \tag{A2}$$

$$E_y|_{z=0} = \frac{\lambda}{2\pi}\frac{1}{\varepsilon+\varepsilon_0} \times \left\{ -\frac{1}{\sqrt{r^2+(y+\ell/2)^2}} + \frac{1}{\sqrt{r^2+(y-\ell/2)^2}} \right\}, \tag{A3}$$

TABLE I. Comparison of the constant C.

Sample	Theory 10^{-14} C	Fitting parameter 10^{-14} C
ethanol	7.4	16
glycerin	4.0	4.9
silicone oil	25	16

$$E_z|_{z=0} = \frac{\lambda}{2\pi r^2}\frac{1}{\varepsilon+\varepsilon_0} \times \left\{ -\frac{a(y+\ell/2)}{\sqrt{r^2+(y+\ell/2)^2}} + \frac{a(y-\ell/2)}{\sqrt{r^2+(y-\ell/2)^2}} \right\}, \tag{A4}$$

where $r^2 \equiv x^2 + a^2$. We consider the surface deformation in place of $y = 0$. The z component of the dielectric force acting on the liquid-air interface is given by [10]

$$P_M = \frac{1}{2}(\varepsilon-\varepsilon_0)\left\{ \left(\frac{\varepsilon}{\varepsilon_0}\right) E_z^2 + E_x^2 + E_y^2 \right\}. \tag{A5}$$

Substituting Eqs. (A2)–(A4) into Eq. (A5) and setting $y = z = 0$, we obtain

$$P_M(x) = \frac{\lambda^2\ell^2}{8\pi^2}\frac{\varepsilon-\varepsilon_0}{(\varepsilon+\varepsilon_0)^2}\frac{1}{(x^2+a^2)^2}\frac{x^2+(\varepsilon/\varepsilon_o)a^2}{x^2+a^2+(\ell/2)^2}. \tag{A6}$$

Note that Eq. (A6) reproduces the representation for a point charge in the limit of $\ell \to 0$, where $q \equiv \lambda\ell$ is constant [11,12].

The constant C in Eq. (3) is therefore given by

$$C = \frac{\lambda^2\ell^2}{8\pi^2}\frac{\varepsilon-\varepsilon_0}{(\varepsilon+\varepsilon_0)^2}. \tag{A7}$$

We estimated the line charge density λ from the applied voltage (375 V) at the edge, and we obtained the value $\lambda = 2.5 \times 10^{-9}$ C/m. The theoretical value calculated by Eq. (A7) is compared with the value obtained by the curve fitting of Fig. 2 in Table I. The agreement is not complete, but it is reasonable.

APPENDIX B: ANALYSIS OF A MODEL FOR THE SKIN LAYER

We use the lubrication approximation to determine the horizontal component of the velocity field $v(x,z,t)$ in the liquid film. Let $p(x,t)$ be the pressure in the liquid at point x. The velocity v satisfies the Stokes equation,

$$\eta\frac{\partial^2 v}{\partial z^2} = \frac{\partial p}{\partial x}. \tag{B1}$$

Let $h(x,t)$ be the profile of the surface. We assume that the equilibrium thickness of the liquid film is h_0 and that the deviation $\zeta(x,t) = h(x,t) - h_0$ is small. The pressure is given by

$$p(x,t) = -\gamma\frac{\partial^2\zeta}{\partial x^2} + \rho g\zeta - P_M(x). \tag{B2}$$

We assume that the surface of the liquid is covered by an elastic membrane. Let $u(x,t)$ be the horizontal displacement

of the membrane. Then the strain of the membrane is given by

$$\epsilon(x,t) = \frac{\partial u}{\partial x}. \tag{B3}$$

The strain causes a restoring force (per unit length)

$$f(x,t) = S\epsilon(x,t), \tag{B4}$$

where S is the elastic constant having the dimension of N/m. (If the thickness of the membrane is b and the shear modulus of the membrane is G, S is approximately given by bG.)

The balance equation for the horizontal force acting on the membrane is written as

$$\frac{\partial f}{\partial x} = \eta \frac{\partial v}{\partial z} \qquad \text{at} \quad z = h_0. \tag{B5}$$

Equation (B1) is solved for the boundary condition of Eq. (B5) and $v(x,0,t) = 0$ to give

$$v(x,z,t) = -\frac{1}{2\eta} p' z(2h_0 - z) + \frac{f'}{\eta} z, \tag{B6}$$

where p' and f' denote $\partial p/\partial x$ and $\partial f/\partial x$, respectively.

The fluid velocity at $z = h_0$ must be equal to the membrane velocity. Hence

$$\frac{\partial u}{\partial t} = v(x,h_0,t) = -\frac{h_0^2}{2\eta} p' + \frac{h_0}{\eta} f'. \tag{B7}$$

The time variation of $h(x,t)$ is obtained from the volume conservation law:

$$\frac{\partial h}{\partial t} = -\int_0^{h_0} \mathrm{d}z \frac{\partial v(x,z,t)}{\partial x}. \tag{B8}$$

Equations (B2)–(B8) give the following set of equations for ζ and ϵ:

$$\frac{\partial \zeta}{\partial t} = \frac{\rho g h_0^3}{3\eta}\left(\frac{\partial^2 \zeta}{\partial x^2} - \kappa^{-2}\frac{\partial^4 \zeta}{\partial x^4}\right) - \frac{S h_0^2}{2\eta}\frac{\partial^2 \epsilon}{\partial x^2} - \frac{h_0^3}{3\eta}\frac{\partial^2 P_M}{\partial x^2}, \tag{B9}$$

$$\frac{\partial \epsilon}{\partial t} = -\frac{\rho g h_0^2}{2\eta}\left(\frac{\partial^2 \zeta}{\partial x^2} - \kappa^{-2}\frac{\partial^4 \zeta}{\partial x^4}\right) + \frac{S h_0}{\eta}\frac{\partial^2 \epsilon}{\partial x^2} + \frac{h_0^2}{2\eta}\frac{\partial^2 P_M}{\partial x^2}, \tag{B10}$$

where κ is the inverse of the capillary length defined in Eq. (5).

The above model considers the fluid flow in the x direction only. According to this model, the integral of ζ over x remains zero unless fluids flow in or out at the edge $x = \pm w/2$. In practice, fluid can flow in or out in the y direction, and the integral of ζ over x is not constant. To account for this effect, we have added a constant term on the right-hand side of Eq. (B9), and we determined the constant by the condition that $\zeta = 0$ at $x = \pm w/2$. The set of equations can be solved easily by Fourier transforms, and the results are given in Sec. V.

[1] J. L. Keddie and A. F. Routh, *Fundamentals of Latex Film Formation* (Springer, Dordrecht, 2010), pp. 95–120.
[2] L. Pauchard and C. Allain, Phys. Rev. E **68**, 052801 (2003).
[3] L. Pauchard and C. Allain, Europhys. Lett. **62**, 897 (2003).
[4] P. G. de Gennes, Eur. Phys. J. E **7**, 31 (2002).
[5] T. Okuzono, K. Ozawa, and M. Doi, Phys. Rev. Lett. **97**, 136103 (2006).
[6] K. Ozawa, T. Okuzono, and M. Doi, Jpn. J. Appl. Phys. **45**, 8817 (2006).
[7] T. Okuzono and M. Doi, Phys. Rev. E **77**, 030501(R) (2008).
[8] I. Ludwig, W. Schabel, M. Kind, J. C. Castaing, and P. Ferlin, AIChE J. **53**, 549 (2007).
[9] K. Sakai and Y. Yamamoto, Appl. Phys. Lett. **89**, 211911 (2006).
[10] *Electrodynamics of Continuous Media*, 2nd ed., edited by L. D. Landau and E. M. Lifshitz (Butterworth-Heinemann, Oxford, 1984), pp. 65–67.
[11] E. Raphaël and P. G. de Gennes, Europhys. Lett. **31**, 293 (1995).
[12] E. Raphaël and P. G. de Gennes, Phys. Rev. E **53**, 3448 (1996).